

# Molecular dynamics simulation and microscopic observation of compatibility and interphase of composited polymer modified asphalt with carbon nanotubes\*

Cai-hua YU<sup>1</sup>, Kui HU<sup>1</sup>, Gui-xiang CHEN<sup>1</sup>, Rong CHANG<sup>†‡2</sup>, Yue WANG<sup>1</sup>

<sup>1</sup>College of Civil Engineering, Henan University of Technology, Zhengzhou 450001, China

<sup>2</sup>Research Institute of Highway Ministry of Transport, Beijing 100088, China

<sup>†</sup>E-mail: r.chang@rioh.cn

Received Aug. 13, 2020; Revision accepted Nov. 29, 2020; Crosschecked June 23, 2021


**Abstract:** Interfacing and compatibility are the most challenging issues that affect the performance of polymer modified asphalt. Mechanisms of interfacial enhancement among four base asphalt components (asphaltenes, resins, aromatics, and saturate), styrene-butadiene-styrene (SBS), and carbon nanotubes (CNTs) were investigated by molecular dynamics simulation, with the aim of understanding the key parameters that control the compatibility of CNTs and interphase behavior on the molecular scale. The compatibility of SBS-modified asphalt (SBSMA) was simulated based on self-assembly theory using indexes of binding energy, mean square displacement, diffusion coefficient, and relative concentration distribution. The interphase behavior and microstructure were observed by fluorescence microscopy and scanning electron microscopy. In addition, a rutting experiment was used to verify the molecular dynamics simulation based on macroscopic performance. The results showed that after adding CNTs, the binding energy of the SBS and aromatics increased from 301.8343 to 327.1102 kcal/mol. The diffusion coefficient of the SBS and asphaltenes decreased more than  $3.2 \times 10^{-11}$  m<sup>2</sup>/s, and the correlation coefficients between the diffusion coefficient and the molecular weight, surface area and volume were all lower than 0.3. Relative concentration distribution curves indicated that CNTs promote the ability of SBS to swell. Microscopic observations demonstrated that the swelling ability of SBS was increased by CNTs. Overall, the interphase of SBSMA was improved by the additional reinforcement, swelling, and diffusion provided by CNTs. Finally, the rutting experiment found that no matter what the temperature, the rutting factor of CNT/SBSMA is higher than that of SBSMA, which corroborates the findings from the molecular dynamics simulations.

**Key words:** Polymer modified asphalt; Carbon nanotubes (CNTs); Molecular dynamics simulation; Microstructure characteristics; Interphase enhancement

<https://doi.org/10.1631/jzus.A2000359>

**CLC number:** U414

<sup>‡</sup> Corresponding author

<sup>\*</sup> Project supported by the Innovative Funds Plan of Henan University of Technology (Nos. 2020ZKCJ05 and 2020ZKCJ22), the Science and Technology Planning Project of Henan Province (No. 192102310229), the Cultivation Plan for Youth Backbone Teachers of Institution of Higher Education by Henan Province (No. 2019GGJS086), the Cultivation Plan for Youth Backbone Teachers by Henan University of Technology, the Key Science and Technology Research Project of Henan Provincial Department of Education (No. 21A580002), the Foundation for Distinguished Young Talents of Henan University of Technology (No. 2018QNJH09), and the Central Public-interest Scientific Institution Basal Research Fund (No. 2020-9049), China  
 ORCID: Cai-hua YU, <https://orcid.org/0000-0003-0494-8117>; Rong CHANG, <https://orcid.org/0000-0002-7591-2413>

© Zhejiang University Press 2021

## 1 Introduction

Styrene-butadiene-styrene (SBS)-modified asphalt accounts for more than 90% of the asphalt used in China. SBS-modified asphalt (SBSMA) is attractive to researchers because of its high-temperature stability, low-temperature crack resistance, and elastic recovery ability (Zhang DM et al., 2018; Slebi-Acevedo et al., 2019; Liu et al., 2020). SBS is the most commonly used polymer to modify asphalt because its polystyrene segment provides strength, while the polybutadiene segment provides elasticity. This combination of

properties can significantly improve the rheological properties of asphalt. Recent studies suggest that when SBS polymers are added to the base asphalt, they will absorb the light components, i.e. aromatics and saturates, and increase the volume by 4 to 10. The swelling SBS forms a 3D physical phagocytic network encompassing the entire asphalt. The excellent performance of SBS polymer is transferred to the base asphalt, and the SBSMA becomes a two-phase structure with a polymer-rich phase and an asphaltene-rich phase. However, the polymer modification is primarily a physical modification, and does not change the chemical composition of SBS and asphalt (Davis and Castorena, 2015; Wang P et al., 2017b). This physical modification process, known as the self-assembly of SBS polymer in base asphalt, gives rise to the excellent performance of SBSMA. However, due to the large differences between SBS polymers and base asphalt including their molecular weight, solubility parameters, polarity, density, and other properties, they are not thermodynamically compatible. At high temperatures, the polymer-rich and asphaltene-rich phases in SBSMA are prone to phase separation (Polacco et al., 2015). This known problem of compatibility between SBS polymer and base asphalt leads to poor stability of SBSMA at high temperatures and therefore restricts its application.

As well as polymers, the addition of nanomaterials is an effective means to enhance asphalt performance due to their large specific surface area and small size (Zhang HL et al., 2018; Khanal et al., 2020; Zeng et al., 2020). Nanomaterials can significantly improve the viscoelastic energy and the high-temperature, anti-aging, anti-fatigue, and moisture-proof performance of asphalt. When dispersed uniformly, nanomaterials can absorb the stress and strain energy of the system caused by external forces and improve the viscosity and temperature stability of asphalt. In addition, due to the formation of large active sites on their surfaces, nanomaterials can chemically bond asphalt molecules and improve the degree of cross-linking, thereby greatly enhancing the ability of asphalt to resist deformation. In summary, nanomaterials have both physical and chemical effects on asphalt (Zhang et al., 2016). Among many nanomaterials, carbon nanotubes (CNTs) (Zhou et al., 2014; Yu et al., 2021) have been most widely used. Wang P et al. (2017a) reported the characteristics of CNTs in SBSMA.

Although current theory can qualitatively describe the effects of modifiers on asphalt, the micro-

scopic mechanisms involved have not been well studied. Various physical techniques including atomic force microscopy, scanning electron microscopy (SEM), Fourier transform infrared spectroscopy (FTIR), and X-ray diffraction can measure the dispersion of the polymers, but the mechanism of interaction between SBS and asphalt is not well understood. Therefore, a study of the microscopic properties of modified asphalt will help to extend our current single-scale understanding and overcome the shortcomings of modified asphalt.

After it was first reported (Zhang and Greenfield, 2007, 2008), many researchers have begun to use molecular simulation to study asphalt materials. Hansen et al. (2013) proposed a four-component model of asphalt, which helped to lay a solid foundation for later studies. Bhasin et al. (2011) verified the self-healing properties of asphalt using molecular dynamics simulations and proposed three indicators that are widely used. After the first Transportation Research Congress summit, there have been numerous reports of molecular modeling methods used to study the properties of asphalt, including interactions between asphalt molecules (Wang et al., 2015), optimization of an asphalt molecular model (Yao et al., 2015, 2016; Lemarchand et al., 2018; Hu et al., 2021), adhesion properties at the asphalt and aggregate interface (Xu and Wang, 2016; Xu et al., 2016; Wang H et al., 2017), self-healing properties of asphalt (Sun et al., 2016), and problems with asphalt aging (Pan and Tarefder, 2016). Some researchers (Xu and Wang, 2016, 2017, 2018) have also introduced binding energy and diffusion coefficients into the asphalt research field.

Although there have been some reports on molecular dynamics, there have been few studies of the macroscopic properties of asphalt materials by molecular dynamics simulation. There have been many reports on the effects of CNTs on the properties of asphalt, but the mechanism of these effects on the molecular motion and interactions of SBSMA systems needs to be studied more systematically.

Herein, we report a molecular dynamics simulation method to simulate the self-assembly behavior of SBSMA and CNT/SBSMA systems. The binding energy, mean square displacement (MSD), diffusion coefficients, and relative concentration distribution of the molecules in SBSMA and CNT/SBSMA systems were determined, and the role of CNTs in the asphalt was analyzed. To verify the simulation results, a rutting experiment was carried out on the two systems.

Electron microscope images of the two systems were obtained by SEM, and fluorescence images were obtained by fluorescence microscopy. Overall, the aim of this study was to construct a bridge between the microstructure and the macroscopic properties of SBSMA, thereby revealing the microscopic mechanisms of modified asphalt.

## 2 Methods

To understand the microscopic mechanisms of the effects of CNTs on SBSMA, it was necessary to select a reasonable molecular model. The interaction behaviors of SBSMA and CNT/SBSMA were analyzed by calculating the binding energy, MSD, correlation coefficient, and relative concentration distribution. Finally, the simulation results were verified by experiments and by measuring the micro morphology.

### 2.1 Model selection and validation

In molecular dynamics simulations, the larger the molecular weight of the system, the more accurate the simulation results, but this comes at the expense of a greater computational cost. Therefore, it is beneficial to find the equilibrium point of calculation amount, calculation time, and molecular weight.

The best method to determine the degree of polymerization in a polymer molecular model is to calculate the solubility parameters of the polymers. When the solubility parameters do not change significantly with the degree of polymerization, an optimal degree of polymerization is considered to have been reached (Fu et al., 2013).

In this study, Materials Studio software was used to construct 21 SBS molecular amorphous cells with different degrees of SBS polymerization, and 24 amorphous cells with different types of CNTs. After 50000 iterations of Geometry Optimization in the Forcite package, each amorphous cell is optimized to reduce the energy to the lowest state. Then, molecular dynamics simulations with 50 ps canonical (NVT) ensemble and 50 ps isothermal-isobaric (NPT) ensemble were carried out. All molecular dynamics simulation parameters were set as follows: the cutoff distance was set as 12.5 Å (1 Å=10<sup>-10</sup> m), spline width was 1 Å, buffer width was 0.5 Å, and charge distribution was in force field assignment. The van der Waals (vdW) interaction in the model was atom-

based, while the electrostatic interaction was Ewald. COMPASS (condensed-phase optimized molecular potentials for atomistic simulation studies) force field was used throughout the study, and all simulated temperatures were set to 298 K.

Amorphous cell snapshots were taken to calculate the solubility parameter  $\delta$  of the last frame. The solubility parameter is defined as the square root of the cohesive energy density (CED), which can be calculated by

$$\delta = \sqrt{\text{CED}} = \sqrt{\frac{E_{\text{coh}}}{V}}, \quad (1)$$

where  $E_{\text{coh}}$  represents the cohesive energy, and  $V$  represents the system volume. The solubility parameters of different SBS polymers and CNTs are shown in Figs. 1 and 2.

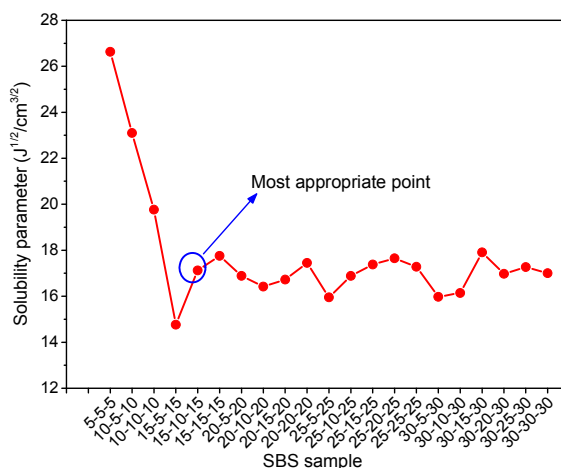


**Fig. 1 Solubility parameters of SBS samples with different degrees of polymerization of S-B-S**

Fig. 1 shows that the solubility parameters of the SBS polymer fluctuate before 15-10-15 and then stabilize. With increasing molecular weight, the parameters first decrease sharply, and then fluctuate around 17 J<sup>1/2</sup>/cm<sup>3/2</sup>, which is consistent with previous results. In other words, when the degree of block polymerization of SBS is greater than the critical value of 15-10-15, the solubility parameters are essentially stable. Therefore, 15-10-15 is the critical degree of polymerization of SBS and was the optimal degree of polymerization for this study.

The solubility parameters of various CNTs are shown in Fig. 2. To save computation resources, the number of repeating units  $l$  was set as 1, 3, or 4. The helical angle  $m$  and the diameter  $n$  were varied from 1

to 8. The solubility parameter of the CNTs first goes down, then stays constant at all repeating units. The stability point is found when the helical angle  $m$  and the diameter  $n$  are both equal to 5. We therefore assume that the number of repeating units has little influence on the solubility parameters of CNTs. Comparing the solubility parameters of the three

CNTs 5-5-1 ( $14.45 \text{ J}^{1/2}/\text{cm}^{3/2}$ ), 5-5-3 ( $14.24 \text{ J}^{1/2}/\text{cm}^{3/2}$ ), and 5-5-4 ( $14.32 \text{ J}^{1/2}/\text{cm}^{3/2}$ ) shows that they are very similar. To reduce the computational cost, the 5-5-1 CNTs were chosen for this study.

The complexity of asphalt means that it is almost impossible to fully understand the molecular composition of asphalt systems. Thankfully, a full understanding is not necessary for most practical applications. Consequently, modern fractional distillation techniques are generally used to separate asphalt into different components. The most well-known is the SARA method, which divides asphalt into the components: saturates (S), aromatics (A), resins (R), and asphaltenes (A).

To establish a more accurate model of asphalt, the quantity of the four components in the model should equal the true values. In this study, the amount of each of the four components of SK90# asphalt was measured by the standard test method (ASTM, 2009), and the results are shown in Table 1. The content of aromatics was the highest at 39.81%. According to modern colloid theory, a higher amount of lighter components will better dissolve the micelles composed of asphaltenes and resins in the system. With a content of 26.83%, resins were the second most abundant in the asphalt, which in modern colloidal theory, is a transition substance between asphaltenes and light components. Although asphaltenes had the lowest content (15.04%), they are the most polar and have the strongest influence on the properties of asphalt.

The molecules in Fig. 3 can accurately describe the asphalt system (Li and Greenfield, 2014). The model of each asphalt molecule is displayed in the Visualizer package of the Materials Studio software, where the calculation of the amorphous cell includes the various molecules, and a molecular model of the asphalt system can be constructed. The model was set to three dimensions, the density to  $1.03 \text{ g}/\text{cm}^3$ , and the temperature to 298 K. Based on this, the SBSMA system model can be constructed by combining the SBS model and CNTs model we obtained.

A neat asphalt system was made in the Amorphous Cell package of Materials Studio by adjusting

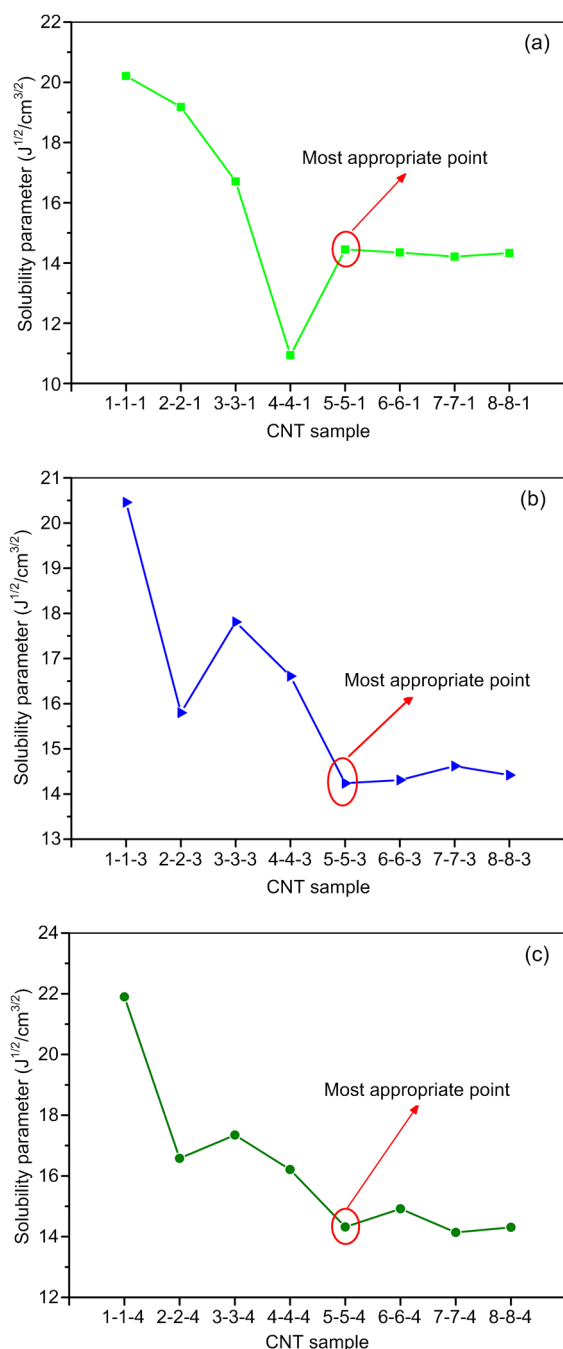


Fig. 2 Solubility parameters of different CNTs ( $m$ - $n$ - $l$ ), with repeating unit numbers of  $l=1$  (a),  $l=3$  (b), and  $l=4$  (c)

Table 1 Proportions of the four fractions in SK90#

Mass (g)	Proportion (%)			
	Asphaltenes	Resins	Aromatics	Saturates
0.24435	15.04	26.83	39.81	18.32

the proportion of each molecule in asphalt to make it conform to the four-component fraction measured by the experiment (Fig. 4). To verify the accuracy of the results, mass fractions of the four components in the model were calculated and compared with the measured values. As shown in Fig. 5, the amount of each of the four components in the model was in good agreement with the measured value, indicating that the model is reliable.

Amorphous cells of the three systems (neat asphalt, SBSMA, and CNT/SBSMA) were established.

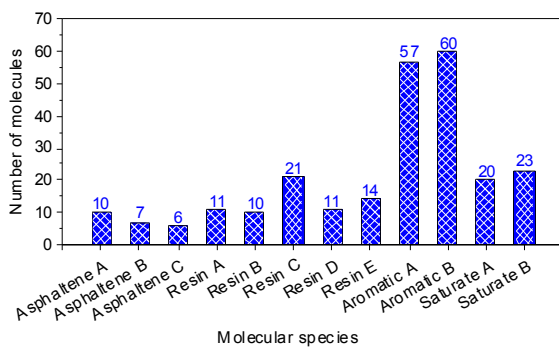


Fig. 4 Numbers of molecules in the asphalt models

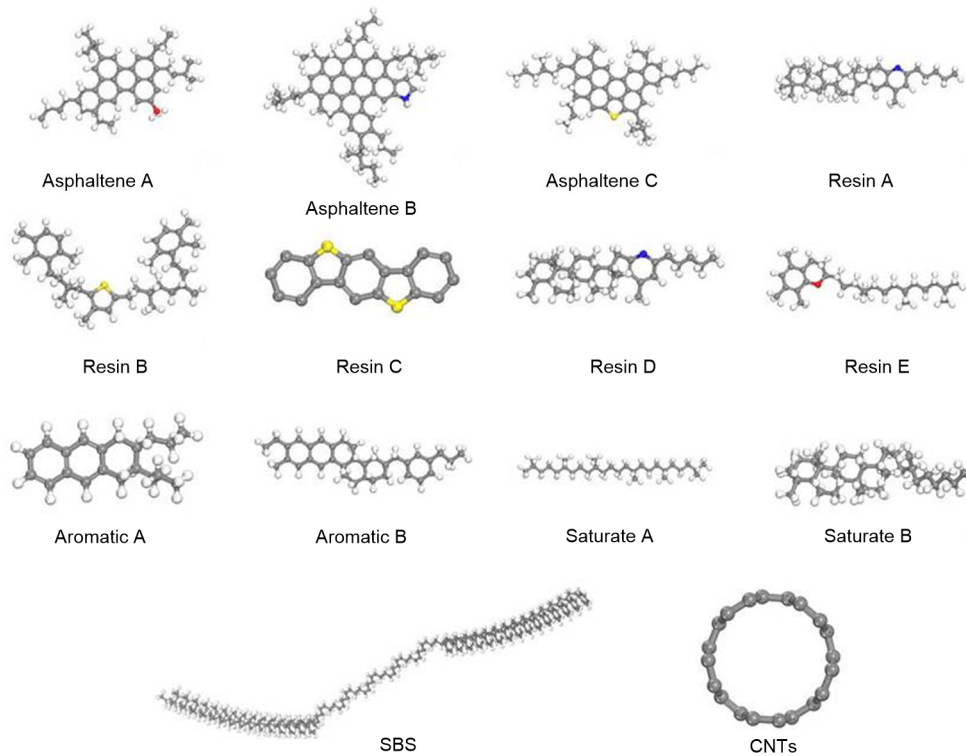


Fig. 3 Four components of asphalt, the optimal SBS molecular chain, and molecular physical model of CNTs. Gray represents C, white represents H, red represents O, blue represents N, and yellow represents S. References to color refer to the online version of this figure

The mass fraction of the SBS polymer was about 6% (mass ratio of SBS in neat asphalt) and the mass fraction of CNTs in CNT/SBSMA was about 0.3% (mass ratio of CNTs to SBSMA). Three kinds of asphalt molecular model systems are shown in Fig. 6. In Fig. 6, red represents asphaltenes, blue represents resins, green represents aromatics, purple represents saturates, gray represents SBS, and black represents CNTs.

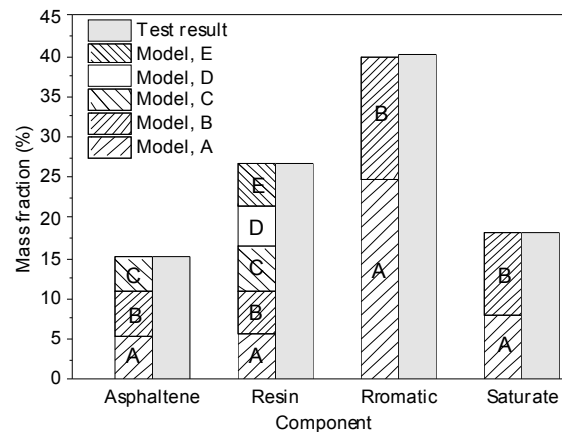
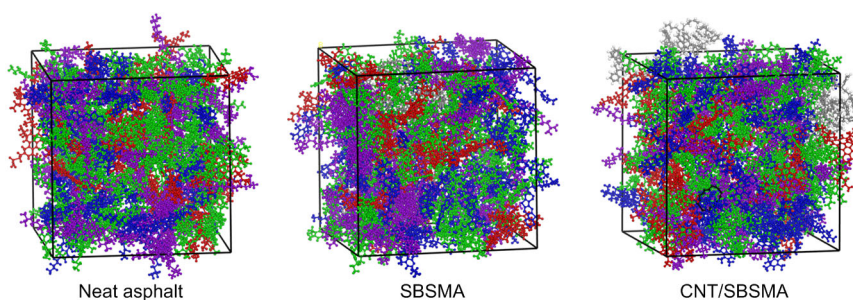


Fig. 5 Calculated proportions and experimental values of the four asphalt components in the simulated system



**Fig. 6** Amorphous cells of the three asphalt systems (red: asphaltenes; blue: resins; green: aromatics; purple: saturates; gray: SBS; black: CNTs). References to color refer to the online version of this figure

To ensure that the simulation method and the resulting data obtained in this study were accurate, the radial distribution function of neat asphalt was calculated. The intramolecular and intermolecular radial distribution functions of neat asphalt are shown in Fig. 7. The intermolecular radial distribution function shows multiple peaks when  $r$  is in the range of 0–4 Å, and the intermolecular radial distribution function  $g(r)$  gradually approaches 0 when  $r \geq 4$  Å. This indicates that the neat asphalt model described in this paper is a short-range ordered and long-range disordered amorphous structure, which is consistent with the microstructure of actual neat asphalt. Through further observation of the intramolecular radial distribution function, we found that the  $g(r)$  value was greater than 0.9 when  $r \geq 4$  Å indicating that the intermolecular interaction of the constructed model was mainly within the range of 8 Å. Normally, the distance range of hydrogen bonding is 0.26–0.31 nm, the range of strong vdW forces is 0.31–0.50 nm, and the range of weak vdW forces is greater than 0.50 nm (Liao et al., 2012). Therefore, the molecular interactions of asphalt in the molecular model are mainly hydrogen bonding and vdW forces, which is consistent with actual asphalt.

The density and solubility parameters of asphalt were calculated and compared with the measured reference values, which are shown in Table 2. The density of the neat model was 1 g/cm<sup>3</sup>, which is close to the lower limit of (1.02±0.02) g/cm<sup>3</sup>. The solubility parameter was 16.66 J<sup>1/2</sup>/cm<sup>3/2</sup>, which is also close to the lower limit reference value of 15.3 J<sup>1/2</sup>/cm<sup>3/2</sup>. The slight difference between the predicted and measured values is likely caused by the presence of impurities in actual asphalt.

Overall, according to the density, solubility parameters, and radial distribution function, the molecular model established in this study has a high degree

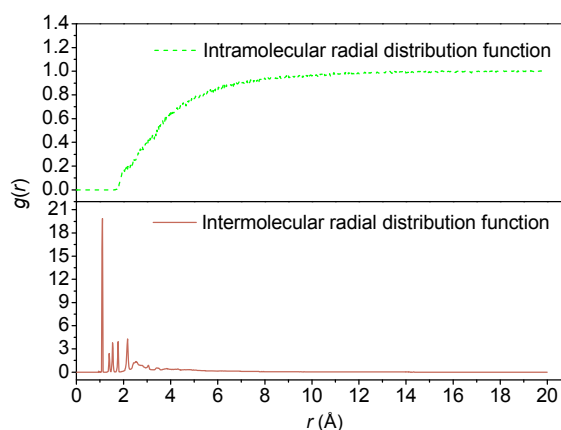


**Fig. 7** Radial distribution functions of neat asphalt

**Table 2** Density and solubility parameters of neat asphalt

Project	Relative density (g/cm <sup>3</sup> )	Solubility parameter (J <sup>1/2</sup> /cm <sup>3/2</sup> )
Neat asphalt model	1.0	16.66
Actual reference value	1.02±0.02	15.3–23.0

of consistency and the resulting simulation results are reliable.

On this basis, a 100-ps molecular dynamics simulation was carried out on all asphalt models under NPT ensemble, at a temperature of 298 K. The simulation used the COMPASS force field, and other sets as described earlier, to analyze the molecular motion and interactions. The classical energy change of the system during the simulation is shown in Fig. 8. After 30 ps, the system completely enters the dynamic equilibrium state.

## 2.2 Several important micro concepts

### 2.2.1 Binding energy

The binding energy  $E_{\text{binding}}$  can well describe the adsorption strength between two substances and is an

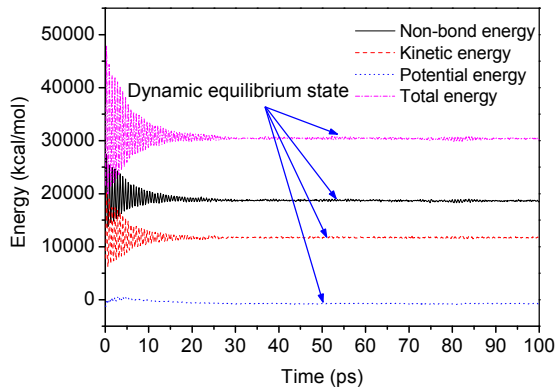


**Fig. 8** Changes of various energies during molecular dynamics simulation

important index used to judge their compatibility.  $E_{\text{binding}}$  is defined as the negative value of the interaction energy  $E_{\text{inter}}$ , which can be calculated using the energy of each component and the total energy of the system. If  $E_{\text{T(AB)}}$  represents the total energy of the A-B system, and  $E_{\text{A}}$  and  $E_{\text{B}}$  represent the energies of A and B, respectively, then  $E_{\text{binding}}$  can be calculated by

$$E_{\text{binding(AB)}} = -E_{\text{inter(AB)}} = E_{\text{A}} + E_{\text{B}}. \quad (2)$$

In the COMPASS force field, the binding energy consists of a bonding and a non-bonding interaction energy:

$$E_{\text{binding(AB)}} = E_{\text{bond}} + E_{\text{non-bond}}, \quad (3)$$

where  $E_{\text{bond}}$  represents the bonding interaction energy, and  $E_{\text{non-bond}}$  represents the non-bonding interaction energy. Non-bonding interactions consist of vdW interaction energy, electrostatic interaction energy, and a long-term correction value:

$$E_{\text{non-bond}} = E_{\text{vdW}} + E_{\text{coulomb}} + E_{\text{lrc}}, \quad (4)$$

where  $E_{\text{vdW}}$  represents the vdW interaction energy,  $E_{\text{coulomb}}$  represents the electrostatic interaction energy, and  $E_{\text{lrc}}$  represents the long range correction.

In the process of calculating the binding energy of asphalt in this study, the excess molecules are initially removed to calculate the total energy of the system, and then each molecule is removed individually to calculate its energy contribution. Then, ac-

ording to the above formulas, the binding energy of SBS and asphalt can be obtained.

### 2.2.2 Mean square displacement and diffusion coefficient

The MSD can represent the diffusion behavior of molecules, and so is an effective method to study molecular diffusion. MSD is defined as the square of the difference between the atomic displacement and the average value of all other atomic displacements. MSD can be calculated by

$$\text{MSD}(t) = \left\langle |r_i(t) - r_i(0)|^2 \right\rangle, \quad (5)$$

where  $\text{MSD}(t)$  represents the MSD at time  $t$ ,  $r_i(t)$  represents the displacement of particle  $i$  at time  $t$ ,  $r_i(0)$  represents the initial displacement of particle  $i$ , and  $\langle \rangle$  represents the average of all particles in the system. The relationship between the diffusion coefficient and MSD is expressed as

$$D = \frac{1}{6} \lim_{t \rightarrow \infty} \frac{d}{dt} \sum_{i=1}^N \left\langle |r_i(t) - r_i(0)|^2 \right\rangle, \quad (6)$$

where  $D$  is the diffusion coefficient of the molecule, and  $N$  is the number of diffusing molecules. In other words, the molecular diffusion coefficient  $D$  is about 1/6 of the slope of the MSD- $t$  curve. However, in a complex system like asphalt, abnormal diffusion is inevitable, so the MSD- $t$  curve cannot be used directly to calculate the diffusion coefficient. In this study, 1/6 of the slope of the  $\lg(\text{MSD})-\lg(t)$  curve in the first 25 ps was selected to calculate the diffusion coefficient.

### 2.3 Preparation and microscopic characterization of modified asphalt

The asphalt used in this study was SK90#. Its technical indicators are given in Table 3. Table 4 shows the technical indicators of the SBS polymer (1301 linear SBS polymer, Sinopec, China) and Table 5 shows the technical indicators of the CNTs (provided by Turing Evolutionary Technologies LTMTM, China).

A sample of asphalt was placed in an oven and heated to a liquid at 175 °C, then 6% SBS polymer was gradually added. The asphalt and SBS mixture was stirred using a high-speed shear mixer at

175–185 °C for 2.5 h at a shear rate of 3000–3500 r/min until the mixture became homogeneous. Then CNTs at 0.3% (in weight) were slowly added to

the SBS/asphalt composite (held at 175–185 °C). After the addition of CNTs, the shear rate of the high-speed shear mixer was maintained at 2000 r/min for 2 h. Using this process, the modified asphalt samples described in this study were obtained. The preparation process is shown in Fig. 9.

**Table 3 Technical indexes of base asphalt**

Physical property	Reference	Measured value
Penetration (25 °C) (mm)	ASTM, 2013	9.05
Penetration index, PI	ASTM, 2013	-1.07
Softening point (R&B) (°C)	ASTM, 2006	47.0
Ductility (15 °C) (cm)	ASTM, 2017	105.2
Kinematic viscosity (135 °C) (Pa·s)	ASTM, 2012	1.027
Density (15 °C) (g/cm <sup>3</sup> )	ASTM, 2003	1.030

**Table 4 Technical indexes of SBS**

Technical index	Description
Ash component (%)	≤0.5
Tensile stress (MPa)	≥2.5
Tensile strength (MPa)	≥12
Elongation (%)	≥700
Shaw hardness (A)	70
Melt flow rate (mm/s)	0.5–6.0
Relative density (23 °C) (g/cm <sup>3</sup> )	0.93

**Table 5 Technical indexes of CNTs**

Technical index	Description
Purity (in weight) (%)	98
Particle size, D <sub>50</sub> (μm)	2–10
Specific surface area (m <sup>2</sup> /g)	50–100
Appearance	Brown powder

The dynamic shear rheometer (DSR) used in the rut experiment was a special DSR which was called SmartPave102 produced by Anton Paar GmbH in Austria. The rut experiment standard was AASHTO T 315-08 (AASHTO, 2008), and the SEM used for measuring the microstructure of the modified asphalt system was a Hitachi S4800 cold-field emission scanning electron microscope. The fluorescence microscope used to observe the microscopic morphology of the SBSMA was a BML-400E type fluorescence detection microscope.

### 3 Results and discussion

#### 3.1 Effects of CNTs on the absorbability of four asphalt components and SBS

The binding energies between the four components of asphalt and SBS polymers were calculated. The results are shown in Table 6, where positive values represent attraction and negative values represent repulsion.

Using the data in Table 6, it can be predicted that non-bonding energy accounts for a significant portion of the binding energy. The extremely small value of the bond energy is a result of the accuracy of

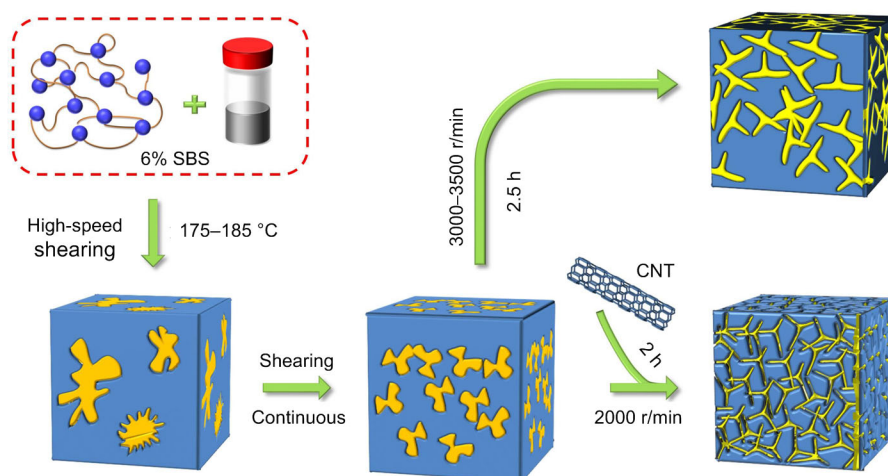


**Fig. 9 Two sample preparation processes**



the software. Therefore, the binding energy is completely attributed to non-bonding energy, which confirms our understanding that SBSMA is primarily a physical modification. In the non-bonding energy, the vdW interaction is the primary component, with electrostatic interaction accounting for only a small proportion of between 0.3% and 6.9%, and sometimes being a negative value. This shows that vdW interaction is the dominant interaction in SBSMA and electrostatic interaction has little effect.

In SBSMA, considering the binding energies of SBS with the four components of asphalt, the binding energy of SBS/aromatics was the highest (301.8343 kcal/mol) followed by SBS/saturates (109.1334 kcal/mol). The binding energy of SBS/resins was smaller (68.8419 kcal/mol), and SBS/asphaltenes had the lowest value (−8.7417 kcal/mol), which indicates that SBS and asphaltenes are mutually exclusive. In other words, the binding strength of SBS with the four components of asphalt decreases in the following order: aromatics>saturates>resins>asphaltenes, which is consistent with previous study (Polacco et al., 2015). In addition, the binding energies of asphaltenes/aromatics (855.2283 kcal/mol) and asphaltenes/saturates (348.4514 kcal/mol) are both significantly higher than those of SBS/aromatics and SBS/saturates. This means that the strength of the interaction between asphaltenes and light components is greater than that of SBS with light components, which may give rise to an insufficient swelling of SBS.

In the CNT/SBSMA, the binding energies of SBS/saturates and asphaltenes/aromatics decreased, but the binding energies between the other components increased. This suggests that the addition of CNTs increased the stability of the SBSMA system. In addition, the binding energy of SBS/asphaltenes was 75.0574 kcal/mol, which was the lowest among the four components, indicating that even with the addition of CNTs, SBS and asphaltenes were highly incompatible. The binding energies of SBS/resins and SBS/aromatics were greatly improved (108.8275 and 25.2759 kcal/mol, respectively). With the addition of CNTs, the interaction between asphaltenes and saturates increased, but interaction between SBS and saturates weakened. Similarly, the interaction between SBS and aromatics was enhanced, but the interaction between asphaltenes and aromatics was weakened. This indicates that CNTs cause a molecular redistribution and promote the swelling of SBS polymers. The process described above is essentially a competition between SBS and asphaltenes for the light components. In other words, the CNTs did not change the competition between SBS and asphaltenes for light components; they simply played a rebalancing role, which is beneficial for the swelling of the SBS polymers.

To further explore the influence of CNTs on the intermolecular interaction strength in SBSMA systems, the statistical significance of the binding energy data was calculated. The two sets of data were input into SPSS software to perform a normality test. It

**Table 6 Binding energies between molecules in SBSMA and CNT/SBSMA systems**

Project	System	Binding energy (kcal/mol)	Bond energy (kcal/mol)	Non-bonding energy (kcal/mol)		
				vdW	Long range correction	Electrostatic
SBS/asphaltenes	SBSMA	−8.7417	0.0003	−17.208	7.286	1.180
	CNT/SBSMA	75.0574	−0.0006	75.173	4.252	−4.367
SBS/resins	SBSMA	68.8419	−0.0001	63.026	4.278	1.538
	CNT/SBSMA	177.6694	0.0004	167.107	7.241	3.321
SBS/aromatics	SBSMA	301.8343	−0.0017	283.427	10.880	7.529
	CNT/SBSMA	327.1102	0.0002	310.612	10.812	5.686
SBS/saturates	SBSMA	109.1334	0.0004	102.777	6.023	0.333
	CNT/SBSMA	93.9555	−0.0005	87.148	5.986	0.822
Asphaltenes/aromatics	SBSMA	855.2283	−0.0017	842.838	23.331	−10.939
	CNT/SBSMA	786.7850	−0.0020	782.526	23.185	−18.924
Asphaltenes/saturates	SBSMA	348.4514	0.0804	345.953	12.917	−10.499
	CNT/SBSMA	431.5328	−0.0012	426.557	12.836	−7.859

was found that  $p$ -value is 0.20 ( $>0.05$ ) in SBSMA and CNT/SBSMA systems. Therefore, it can be assumed that the two sets of binding energy data obeyed a normal distribution. An independent sample  $T$ -test was performed on the two sets of data, which gave a significance of 0.25 ( $>0.05$ ), indicating that the difference in binding energy between the two groups was not significant. In other words, the addition of CNTs to the SBSMA system did not significantly change the molecular interactions. This is likely because SBS is thermodynamically incompatible with asphalt, and the interaction between them can be achieved only in an engineering sense. The modification of asphalt by SBS is simply a physical change, and intermolecular interaction is therefore not strong. Although CNTs will change the intermolecular interaction in the SBSMA system to a certain extent, the change will not fundamentally alter the fact that the interaction between SBS and asphalt is weak.

The interaction morphologies of the six molecular groups in the SBSMA system were studied. SBS and asphaltenes are independent clusters and show entanglement (Fig. 10a), which indicates that the interaction of SBS/aromatics is weak and their compatibility is poor. From the calculated interaction morphology of SBS/resins (Fig. 10b), we found that one SBS molecular chain can be surrounded by resin molecules while others can be found far from the resin molecules. This suggests that the interaction of SBS/resins is stronger than that of SBS/asphaltenes, but they still do not result in swelling of the SBS, and their overall compatibility with SBS is poor. SBS and aromatics (Fig. 10c), however, were found to fully cross-link with each other as numerous aromatics bind to the SBS chain. This interaction will cause SBS to swell and promote the formation of a 3D network. Moreover, it indicates that the compatibility of SBS with aromatics is excellent. Saturates were similarly absorbed by SBS (Fig. 10d), but there were fewer saturate molecules found between the SBS polymer chains, and the cross-link with SBS was weak. Therefore, the cross-linking entanglements of saturates with SBS are weaker than those of aromatics, but stronger than those of asphaltenes and resins. Note that the interactions of asphaltenes/aromatics (Fig. 10e) and asphaltenes/saturates (Fig. 10f) are defined by deep cross-linking. Because of the variety and quantity of asphaltenes, the contact surface area

of asphaltenes is larger, suggesting that asphaltenes are more likely to interact with light components than the SBS polymers.

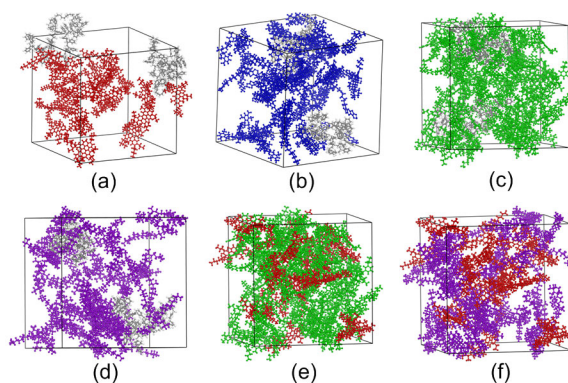


**Fig. 10 Morphologies of intermolecular interactions** (a) SBS/asphaltenes; (b) SBS/resins; (c) SBS/aromatics; (d) SBS/saturates; (e) Asphaltenes/aromatics; (f) Asphaltenes/saturates

### 3.2 Effects of CNTs on SBS diffusion ability in base asphalt

The MSD curves of various molecules in SBSMA and CNT/SBSMA are shown in Fig. 11.

Fig. 11 shows that the order of the diffusion rates of the molecules in the SBSMA system ranged from fastest to slowest according to the following trend: resin C>saturate B>resin B>resin A>saturate A>SBS>asphaltene B>aromatic B>resin E>asphaltene C>aromatic A>asphaltene A>resin D. The diffusion rates of the three asphaltenes were relatively slow in the SBSMA system. The diffusion rates of the resin molecules were widely distributed, with resin C being the fastest diffusing molecule in the system, and resin D the slowest, suggesting that the resins are very active. This activity arises because resins are a transition substance between asphaltenes and light components. Moreover, the asphaltenes are numerous and well dispersed, so to adhere to the asphaltene periphery, the diffusion rate distribution of resins needs to be very wide. However, the order of diffusion rates of various molecules in the CNT/SBSMA system from highest to lowest was: resin B>resin D>resin C>saturate A>aromatic A>aromatic B>resin E>asphaltene B>saturate B>SBS>asphaltene C>asphaltene A>resin A. The addition of CNTs significantly changed the diffusion rates of various molecules and caused a redistribution of the molecules

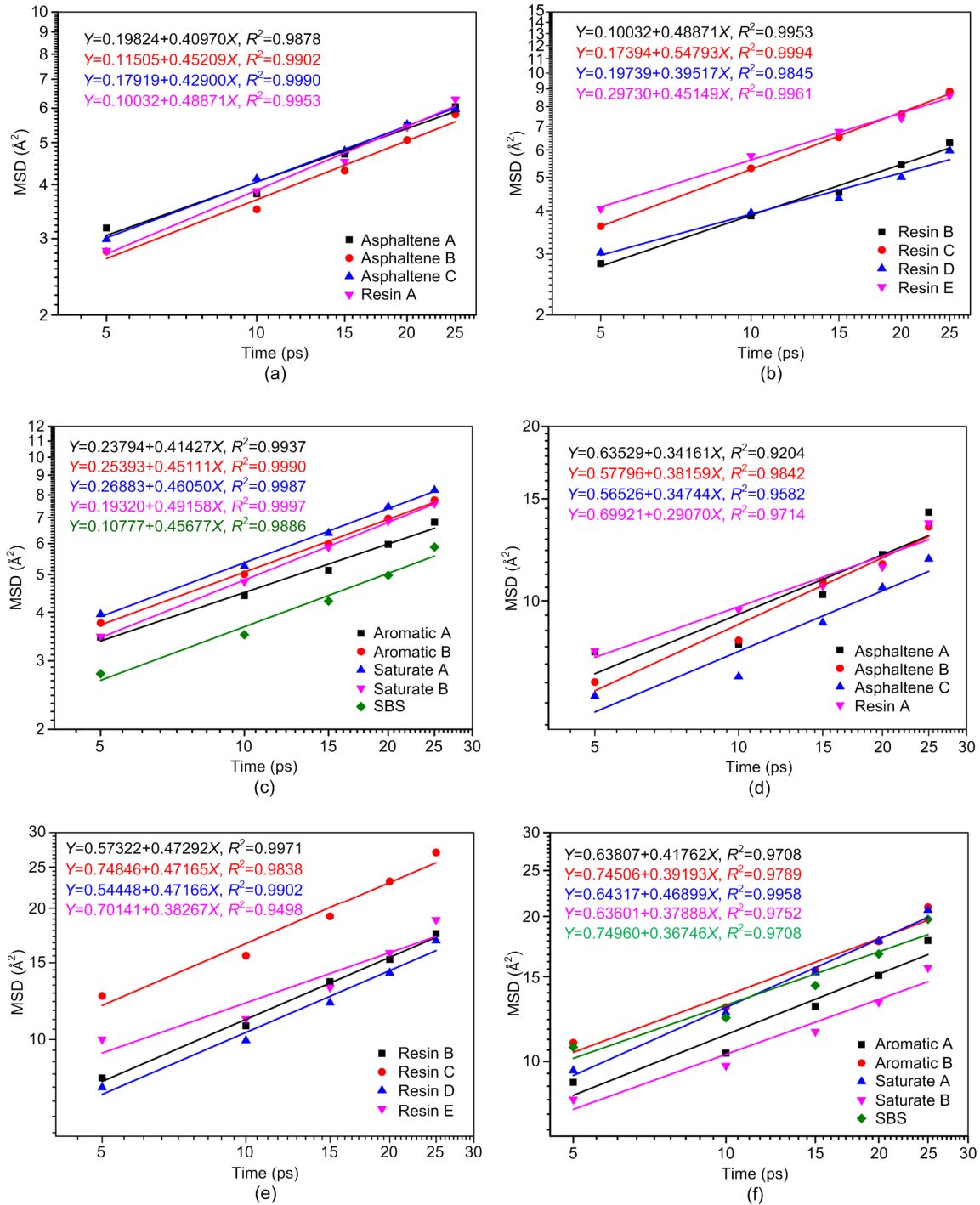


Fig. 11 MSD and linear regression curves of various molecules in the two systems: (a)-(c) SBSMA system; (d)-(e) CNT/SBSMA system. References to color refer to the online version of this figure

in the SBSMA system. Diffusion rates of various molecules in SBSMA and CNT/SBSMA systems were not easily predicted by any known trend.

To further investigate the role of CNTs in SBSMA, a linear regression analysis was performed

on the  $\lg(\text{MSD})-\lg(t)$  curve, and the following were calculated: diffusion coefficients for each molecule, and the correlation coefficients between the diffusion coefficients and the molecular weight, surface area, and volume. The calculated diffusion coefficients are

shown in Fig. 12. Note that the molecular surface areas and volumes in this study were calculated in Materials Studio software by creating a study table document, inserting the molecules to be calculated, and then selecting the properties to be calculated in models.

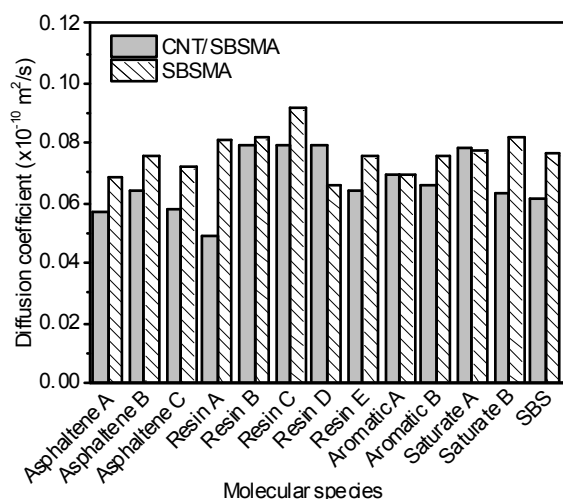


**Fig. 12** Diffusion coefficients of various molecules in both systems

From Fig. 11, most values of  $R^2$  were greater than 0.95, indicating that the linear relationship between  $\lg(\text{MSD})$  and  $\lg(t)$  in the two systems was accurate and the calculated diffusion coefficients were reliable. As shown in Fig. 12, the diffusion coefficients in the CNT/SBSMA system were lower than those in the SBSMA system, indicating that the addition of CNTs inhibited the diffusion of various molecules in the system. This is likely related to the simulation results of the binding energy. The binding energy between various molecules in CNT/SBSMA was generally higher than that of the system without CNTs, and the binding in the system will limit the diffusion of molecules. In the SBSMA system, the binding energies were low, so the movement of each molecule was relatively unhindered, which is demonstrated by the high diffusion coefficient. In addition, the diffusion coefficients of various molecules in the CNT/SBSMA were similar to each other. This equal diffusion could promote the uniform distribution of various molecules in the system and contribute to its stability.

The molecular weight, surface area, and volume

of various molecules are shown in Table 7, and the correlation coefficients are shown in Fig. 13.

**Table 7** Molecular weight, surface area and volume of various molecules

Molecule	Molecular weight	Surface area ( $\text{\AA}^2$ )	Volume ( $\text{\AA}^3$ )
Asphaltene A	577	1010	1850
Asphaltene B	861	1290	2500
Asphaltene C	707	1160	2140
Resin A	558	885	1640
Resin B	545	985	1780
Resin C	280	464	738
Resin D	504	798	1480
Resin E	401	845	1450
Aromatic A	465	847	1490
Aromatic B	266	536	906
Saturate A	423	943	1630
Saturate B	483	762	1430
SBS	3670	4040	8660

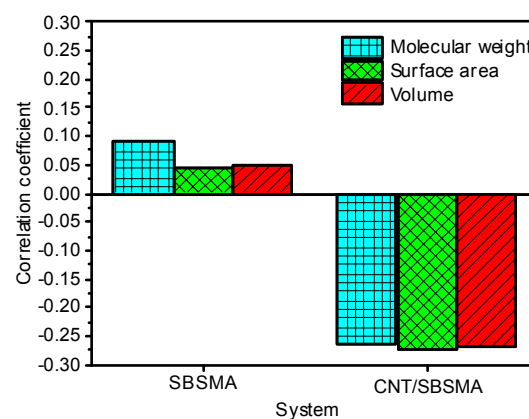


**Fig. 13** Correlation coefficients between the diffusion coefficient and the molecular weight, surface area, and volume in the two systems

As shown in Fig. 13, the correlation coefficient between the diffusion coefficient and the molecular weight of the SBSMA system was about 0.088, the correlation coefficient with surface area was about 0.049, and the correlation coefficient with volume was about 0.051. These correlation coefficients are less than 0.1, which are very low. However, in the CNT/SBSMA system, the corresponding correlation coefficients were  $-0.264$ ,  $-0.284$ , and  $-0.272$ , respectively. Note that the correlation coefficients of the CNT/SBSMA system were significantly greater than those of SBSMA system. This indicates that the diffusion

coefficients of the CNT/SBSMA system are affected by the molecular surface area, where the influences of molecular weight and volume are higher. The reason for this is that CNTs promote a stronger interaction between molecules, causing a slower molecular motion. Therefore, the kinetic energy is reduced, and the molecular weight of the molecules and the influences of the surface area and volume will be magnified.

From the above analysis, the surface area, molecular weight, and volume of molecules have no significant effect on the diffusion of molecules in the system. The strongest influence on the diffusion of molecules is the interaction between molecules in the system.

### 3.3 Effects of CNTs on various molecular concentration distributions

The last frame of the molecular dynamics simulation of the two systems was to calculate the relative concentration (mass concentration) distribution of each molecule. The concentration distribution of various molecules of the SBSMA system in the *X*-direction is shown in Fig. 14a, the concentration distribution in the *Y*-direction is shown in Fig. 14b, and the concentration distribution in the *Z*-direction is shown in Fig. 14c. To interpret these observations, we have denoised the curves using Origin software (Sun and Wang, 2020).

In Fig. 14a, asphaltenes, resins, and SBS show intense peaks, indicating that they are aggregated in the system. Aromatics and saturates show smaller peaks, indicating that they are more evenly distributed. Further inspection of the distribution intervals of various molecular peaks reveals that asphaltenes are always flanked by resin molecules, saturates, or aromatics. In other words, asphaltenes have an obvious adsorption affinity to resins to form micelles, which are surrounded by aromatic and saturate fractions. This is consistent with colloid theory. Although the peak amplitudes of the aromatics and saturates are small, they are obviously distributed on both sides of the SBS polymers, suggesting an adsorption effect between SBS and light components. This aligns with the current understanding that SBS expands by absorbing the light components in asphalt. Further analysis revealed that there was a peak attributed to asphaltenes in the same region as the SBS peak, right between the peaks of aromatics and saturates, indi-

cating that both SBS and asphaltenes adsorbed aromatic and saturate molecules in this range. In other words, SBS will compete with asphaltenes for light components, which may lead to insufficient swelling of SBS and affect the performance of SBSMA.

In Fig. 14b, there are two peaks associated with SBS with the asphaltene peaks sandwiched between them, while the light components are evenly distributed. This indicates that SBS is in fierce competition with asphaltenes. Fig. 14c further indicates the colloidal structure theory of asphalt, with SBS in competition with asphaltenes for light components. Fig. 14c shows that after each asphaltene peak, there is a clear transition between asphaltenes and resins, indicating the adsorption of asphaltenes and resins.

The relative concentration distribution of various molecules was calculated in all directions of the CNT/SBSMA system. The concentration distribution in the *X*-direction is shown in Fig. 15a (p.542), the concentration distribution in the *Y*-direction in Fig. 15b, and the concentration distribution in the *Z*-direction in Fig. 15c.

According to Fig. 15a, compared with SBSMA, the distribution of aromatics and saturates in the CNT/SBSMA system is more uniform and the peaks are not obvious. However, SBS is surrounded by light components, which allows the SBS to swell. Several asphaltene peaks interweave to form one large peak and are surrounded by resin peaks. Taken together, these phenomena indicate that the CNT/SBSMA system is more stable than the SBSMA system, and the SBS swelling is higher. In other words, CNTs can promote the swelling of SBS, and improve the stability and performance of SBSMA. CNTs, however, did not change the colloid structure of the SBSMA, rather they just caused a rebalancing of the colloid structure. Note that this rebalancing does not eliminate the competition, but the inadequate swelling of the SBS is relieved due to the uniform distribution of aromatics and saturates.

Fig. 15b shows that the distribution of resins is uniform and there is an alternating pattern of peaks that helps to alleviate the conflict between asphaltenes and SBS. When compared with the SBSMA, the number of peaks in the concentration distribution curve in the CNT/SBSMA is significantly reduced. This means that the distribution of various molecules in the system is relatively uniform. By combining the

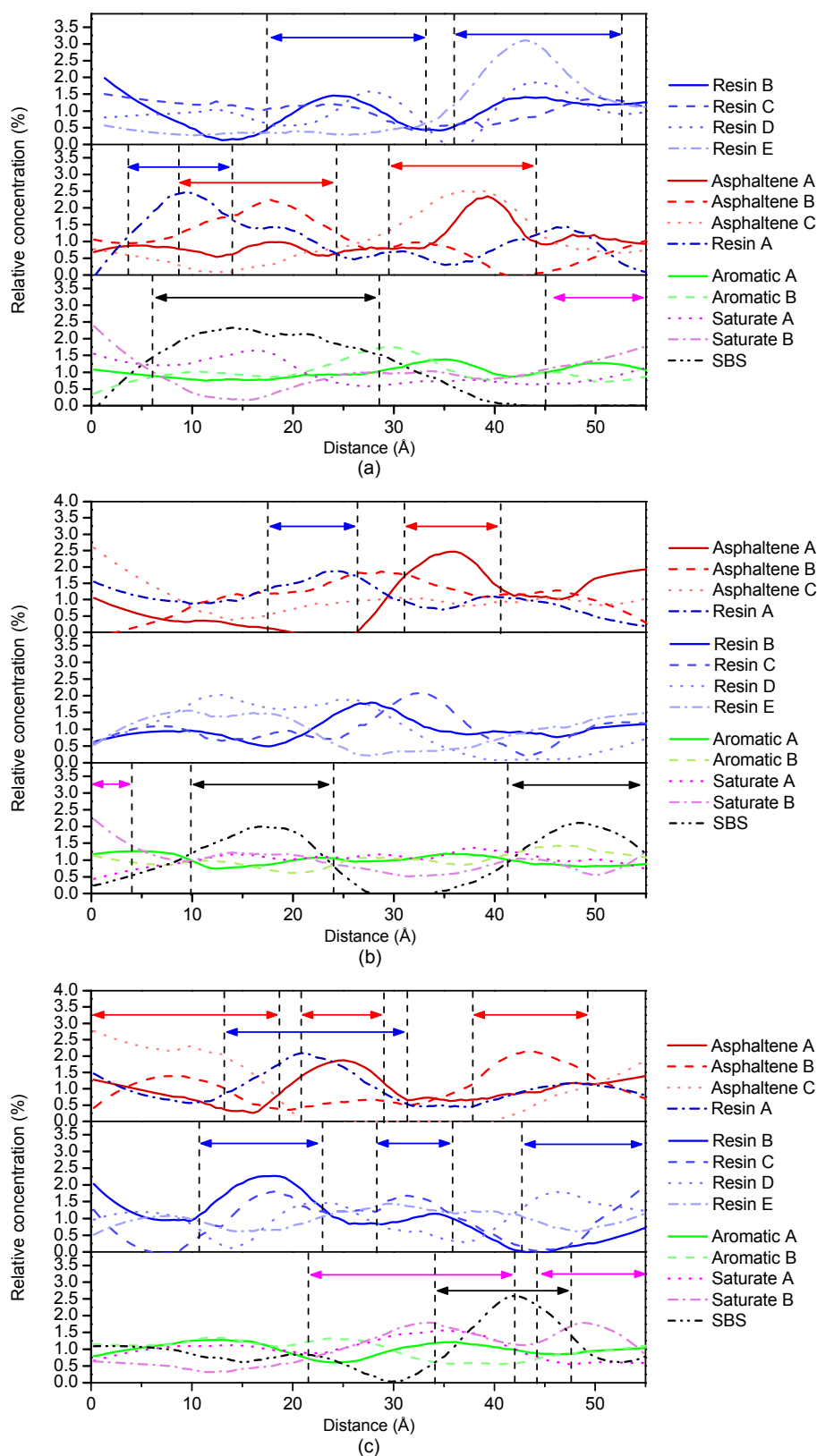


**Fig. 14** Relative concentration distributions of SBSMA molecules: (a) X-direction; (b) Y-direction; (c) Z-direction (red arrow represents the peak asphaltenes distribution region, blue represents resin, green represents aromatic, purple represents saturate, and black represents SBS). References to color refer to the online version of this figure

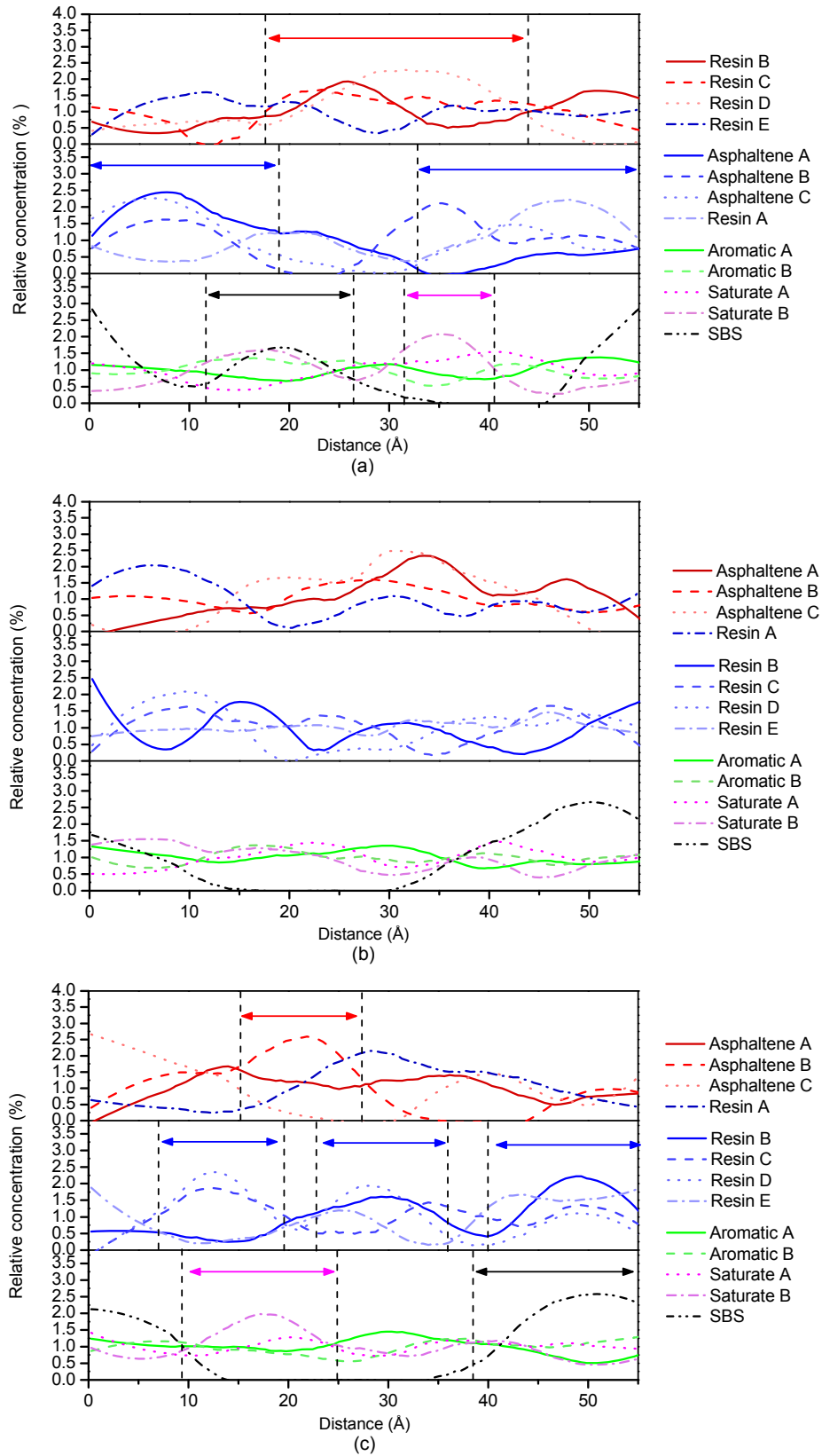


**Fig. 15** Relative concentration distributions of CNT/SBSMA molecules: (a) X-direction; (b) Y-direction; (c) Z-direction. References to color refer to the online version of this figure

simulation results of the MSD and the binding energy, we found that the addition of CNTs strengthens the interaction between various molecules in the system, thereby slowing down the movement of molecules and reducing the diffusion coefficient. However, slow molecular diffusion not only causes the aggregation of SBS polymers, but also increases the swelling of SBS. Overall, CNTs guide the movement of various molecules in the SBSMA system and therefore make the system more stable. The above conclusions are also supported by the results shown in Fig. 15c.

### 3.4 Rutting properties and micromorphology of two kinds of modified asphalt

The calculation of the rutting factor in this study is given in Fig. 16. Within the temperature range of 58–76 °C, the rutting factors of both the SBSMA and CNT/SBSMA samples decreased with increasing temperature, and the slope of the curve became shallower. Therefore, temperature has a significant influence on the rutting factor of modified asphalt and increasing temperature is detrimental to the pavement performance of modified asphalt. Moreover, with increasing temperature, the rutting factor decreases gradually.

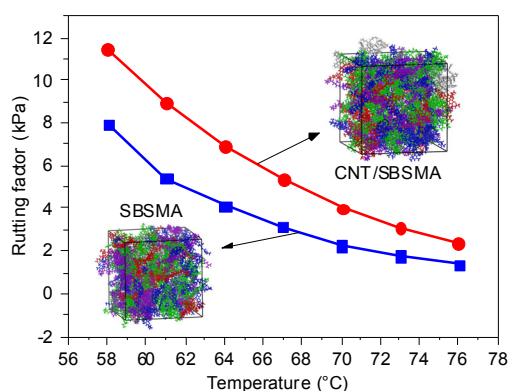


**Fig. 16** Rutting factors of SBSMA and CNT/SBSMA at different temperatures. References to color refer to the online version of this figure

For SBSMA, when the temperature is greater than 70 °C, the rutting factor is close to 0. From an engineering point of view, the practicability of SBSMA is very low because of the separation of the polymer-rich and asphaltene-rich phases. For CNT/SBSMA, regardless of the temperature, the rutting factor was significantly higher than that of the SBSMA (with an increase of 44.1%–75.4%). However, with increasing

temperature, the two curves gradually coalesce, indicating that high temperature has an impact on the performance of all SBSMAs. Even the addition of CNTs cannot prevent the failure of SBSMA at high temperatures, so modified asphalt should be avoided in high-temperature environments.

Rutting factor enhancement is closely related to the self-assembly of SBS in base asphalt, and the rutting factor of SBSMA after adding CNTs was increased. According to the results of the molecular dynamics simulation, the CNT/SBSMA rutting factor is higher than that of SBSMA. A possible explanation for this result is that the addition of CNTs improves the binding energy of SBS and asphalt.

The micromorphology of SBSMA and CNT/SBSMA was observed by SEM. SEM images of SBSMA and CNT/SBSMA systems are shown in Fig. 17. The CNTs (Fig. 17a) are a block with sharp edges and a large surface area. The ordinary SBSMA (Fig. 17b) contains obvious banded SBS polymers, which are aggregated, so SBS polymers are not observed in a considerable portion of the asphalt. This degree of aggregation and uneven distribution of SBS polymers in the ordinary SBSMA reduces the ability of SBS polymers to fully swell, which greatly affects the performance of SBSMA. No obvious SBS aggregation was observed in CNT/SBSMA (Fig. 17c), but there was obvious CNT aggregation. Although there was aggregation in the CNT/SBSMA, the SBS polymers were fully swollen and uniformly distributed in the base asphalt, which is beneficial to pavement performance. In other words, CNTs will promote the uniform distribution of SBS polymers which can be swollen by light components in the base asphalt, thus forming a better physical phagocytic network. However, CNTs are prone to aggregation due to their large specific surface area, which becomes a more serious concern when the mass fraction of CNTs is 1.0% (Fig. 17d).

Fluorescence microscope images of SBSMA and CNT/SBSMA are shown in Fig. 18. In SBSMA (Fig. 18a), the SBS polymer is flocculent and tends to be interconnected in a network. The SBS has an effect on the asphalt, but the network formed in SBSMA is not stable. However, after the addition of CNTs (Fig. 18b), the SBS polymer formed an obvious 3D network structure, which suggests good stability. In addition, the distance between SBS units in CNT/SBSMA was significantly smaller than that observed



in SBSMA. Therefore, the molecular movement of CNT/SBSMA in the system was weaker than that of SBSMA, which was consistent with the simulation results.

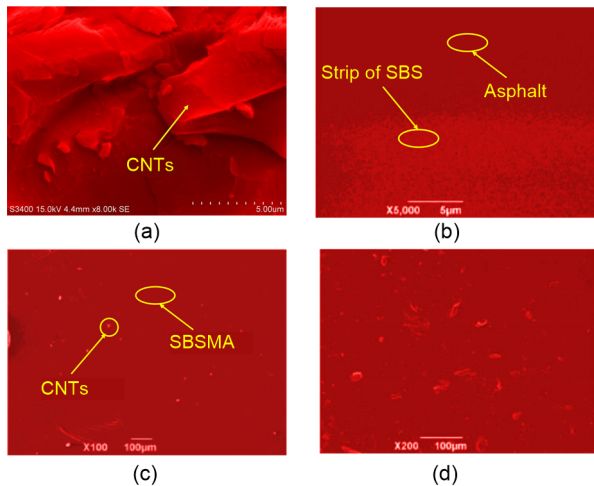


**Fig. 17** SEM images of SBSMA and CNT/SBSMA samples (a) CNTs; (b) SBSMA; (c) 0.3% CNT/SBSMA; (d) 1.0% CNT/SBSMA

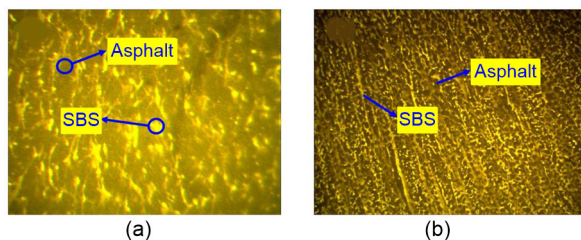


**Fig. 18** Fluorescence microscopic images (yellow represents SBS and dark represents asphalt): (a) SBSMA; (b) CNT/SBSMA. References to color refer to the online version of this figure

The above rutting tests, and SEM and fluorescence microscope observations are consistent with the results of the molecular dynamics simulation of the binding energy, diffusion coefficients, and relative concentration distribution. The molecular dynamics method used in this study is therefore effective for simulating the effect of CNTs on the self-assembly of SBS polymers in base asphalt.

## 4 Conclusions

To study the effect of CNTs on the self-assembly of SBS polymers in base asphalt, molecular models of SBSMA and CNT/SBSMA were constructed. This

was accomplished by modeling the asphalt components. The binding energy, diffusion coefficient, and relative concentration distribution of various molecules in the two systems were calculated. The effects of CNTs were analyzed and the following conclusions were drawn.

The impact of SBS on asphalt is mainly a physical modification. The molecular interaction in the system is mainly van der Waals bonding, and electrostatic interaction is relatively weak. The addition of CNTs greatly increased the binding energies of various molecules in asphalt with SBS polymers, which made the system more stable. The morphology of the interaction between SBS and asphalt was further analyzed, and the compatibility of SBS with aromatics and saturates was found to be high as the molecules intertwined with each other. However, asphaltenes were also intertwined with aromatics and saturates, indicating that SBS will compete with asphaltenes for these light components in the asphalt system, which may result in inadequate SBS swelling. A *T*-test was performed on the binding energy of the two modified asphalt systems. Both data sets showed a normal distribution, and the difference between them was not statistically significant. This means that CNTs did not impact the weak interaction between SBS and asphalt.

The MSD curves of various molecules in the two systems were obtained and their diffusion coefficients were calculated. CNTs decreased the diffusion coefficient of each molecule in the asphalt systems. The correlation coefficients between the diffusion coefficient and the molecular weight, surface area, and volume were calculated, and it was found that CNTs increased the absolute value of the correlation coefficients. However, the correlation coefficients with molecular weight, surface area, and volume were still low, less than 0.3. This indicates that the diffusion of various molecules in the asphalt system is not significantly affected by surface area, molecular weight, or volume, but depends mainly on the interaction between molecules in the system.

Relative concentration distribution curves were analyzed to verify the colloid structure theory that SBS will compete with asphaltenes for aromatics and saturates. The competition is fierce. However, the addition of CNTs makes the distribution of aromatics and saturates more uniform, alleviating the competition between SBS and asphaltenes, thereby promoting

the swelling of SBS. Thus, CNTs inhibited the diffusion of various molecules in the system, but guided the movement of various molecules, thereby increasing the stability of the system.

Samples of SBSMA and CNT/SBSMA were prepared and a rut test was conducted. CNTs were found to enhance the rutting factor of SBSMA at various temperatures (growth was between 44.1% and 75.4%). The microscopic morphology of SBSMA and CNT/SBSMA samples was observed using SEM. CNTs caused the SBS distribution to be more uniform and the SBS polymers to fully swell. SEM and fluorescence microscopy were used to observe the micro-morphologies of the two systems, which matched well with the molecular dynamics simulation results. The experimental results agreed well with the simulation data indicating that the molecular dynamics simulation of the self-assembly of SBSMA used in this study is reliable.

The difficulty in studying modified asphalt is that it is an extremely complex system, containing millions of molecules and various impurities, and the composition of asphalt from different sources is wildly variable. Therefore, even after many researchers have studied asphalt, there is no universal law. The limitation of this study is that only 12 kinds of molecules were used to represent the asphalt system. Although 12 is larger than the numbers used in previous asphalt models, this still far from accurately represents the complexity and randomness of asphalt. There is an opportunity for further development of this complex system by chemists.

### Contributors

Cai-hua YU designed the research. Kui HU and Rong CHANG processed the corresponding data. Cai-hua YU wrote the first draft of the manuscript. Kui HU and Rong CHANG helped to organize the manuscript. Gui-xiang CHEN and Yue WANG revised and edited the final version.

### Conflict of interest

Cai-hua YU, Kui HU, Gui-xiang CHEN, Rong CHANG, and Yue WANG declare that they have no conflict of interest.

### References

AASHTO (American Association of State Highway and Transportation Officials), 2008. Standard Method of Test for Determining the Rheological Properties of Asphalt Binder Using a Dynamic Shear Rheometer (DSR), AASHTO T 315-08. AASHTO, USA.

ASTM (American Society for Testing and Materials), 2003. Standard Test Method for Density of Semi-solid Bitu-

minous Materials, ASTM D70-03. ASTM International, USA.

ASTM (American Society for Testing and Materials), 2006. Standard Test Method for Softening Point of Bitumen (Ring-and-Ball Apparatus), ASTM D36-06. ASTM International, USA.

ASTM (American Society for Testing and Materials), 2009. Standard Test Method for Separation of Asphalt into Four Fractions, ASTM D4124-09. ASTM International, USA.

ASTM (American Society for Testing and Materials), 2012. Standard Test Method for Viscosity Determination of Asphalt at Elevated Temperatures Using a Rotational Viscometer, ASTM D4402/D4402M-12. ASTM International, USA.

ASTM (American Society for Testing and Materials), 2013. Standard Test Method for Penetration of Bituminous Materials, ASTM D5/D5M-13. ASTM International, USA.

ASTM (American Society for Testing and Materials), 2017. Standard Test Method for Ductility of Asphalt Materials, ASTM D113-17. ASTM International, USA.

Bhasin A, Bommavaram R, Greenfield ML, et al., 2011. Use of molecular dynamics to investigate self-healing mechanisms in asphalt binders. *Journal of Materials in Civil Engineering*, 23(4):485-492.  
[https://doi.org/10.1061/\(ASCE\)MT.1943-5533.0000200](https://doi.org/10.1061/(ASCE)MT.1943-5533.0000200)

Davis C, Castorena C, 2015. Implications of physico-chemical interactions in asphalt mastics on asphalt microstructure. *Construction and Building Materials*, 94:83-89.  
<https://doi.org/10.1016/j.conbuildmat.2015.06.026>

Fu YZ, Liao LQ, Yang LX, et al., 2013. Molecular dynamics and dissipative particle dynamics simulations for prediction of miscibility in polyethylene terephthalate/poly lactide blends. *Molecular Simulation*, 39(5):415-422.  
<https://doi.org/10.1080/08927022.2012.738294>

Hansen JS, Lemarchand CA, Nielsen E, et al., 2013. Four-component united-atom model of bitumen. *Journal of Chemical Physics*, 138(9):094508.  
<https://doi.org/10.1063/1.4792045>

Hu K, Yu CH, Yang QL, et al., 2021. Multi-scale enhancement mechanisms of graphene oxide on styrene-butadiene-styrene modified asphalt: an exploration from molecular dynamics simulations. *Materials & Design*, 208:109901.  
<https://doi.org/10.1016/j.matdes.2021.109901>

Khanal LR, Sundararajan JA, Qiang Y, 2020. Advanced nanomaterials for nuclear energy and nanotechnology. *Energy Technology*, 8(3):1901070.  
<https://doi.org/10.1002/ente.201901070>

Lemarchand CA, Greenfield ML, Dyre JC, et al., 2018. ROSE bitumen: mesoscopic model of bitumen and bituminous mixtures. *The Journal of Chemical Physics*, 149(21):214901.  
<https://doi.org/10.1063/1.5047461>

Li DD, Greenfield ML, 2014. Chemical compositions of improved model asphalt systems for molecular simulations. *Fuel*, 115:347-356.  
<https://doi.org/10.1016/j.fuel.2013.07.012>

Liao RJ, Zhu MZ, Zhou X, et al., 2012. Molecular dynamics

- study of the disruption of H-bonds by water molecules and its diffusion behavior in amorphous cellulose. *Modern Physics Letters B*, 26(14):1250088. <https://doi.org/10.1142/S0217984912500881>
- Liu SJ, Zhou SB, Peng AH, 2020. Analysis of moisture susceptibility of foamed warm mix asphalt based on cohesion, adhesion, bond strength, and morphology. *Journal of Cleaner Production*, 277:123334. <https://doi.org/10.1016/j.jclepro.2020.123334>
- Pan JL, Tarefder RA, 2016. Investigation of asphalt aging behaviour due to oxidation using molecular dynamics simulation. *Molecular Simulation*, 42(8):667-678. <https://doi.org/10.1080/08927022.2015.1073851>
- Polacco G, Filippi S, Merusi F, et al., 2015. A review of the fundamentals of polymer-modified asphalts: asphalt/polymer interactions and principles of compatibility. *Advances in Colloid and Interface Science*, 224:72-112. <https://doi.org/10.1016/j.cis.2015.07.010>
- Slebi-Acevedo CJ, Lastra-González P, Pascual-Muñoz P, et al., 2019. Mechanical performance of fibers in hot mix asphalt: a review. *Construction and Building Materials*, 200:756-769. <https://doi.org/10.1016/j.conbuildmat.2018.12.171>
- Sun DQ, Lin TB, Zhu XY, et al., 2016. Indices for self-healing performance assessments based on molecular dynamics simulation of asphalt binders. *Computational Materials Science*, 114:86-93. <https://doi.org/10.1016/j.commatsci.2015.12.017>
- Sun W, Wang H, 2020. Moisture effect on nanostructure and adhesion energy of asphalt on aggregate surface: a molecular dynamics study. *Applied Surface Science*, 510:145435. <https://doi.org/10.1016/j.apsusc.2020.145435>
- Wang H, Lin EQ, Xu GJ, 2017. Molecular dynamics simulation of asphalt-aggregate interface adhesion strength with moisture effect. *International Journal of Pavement Engineering*, 18(5):414-423. <https://doi.org/10.1080/10298436.2015.1095297>
- Wang P, Dong ZJ, Tan YQ, et al., 2015. Investigating the interactions of the saturate, aromatic, resin, and asphaltene four fractions in asphalt binders by molecular simulations. *Energy & Fuels*, 29(1):112-121. <https://doi.org/10.1021/ef502172n>
- Wang P, Dong ZJ, Tan YQ, et al., 2017a. Identifying the rheological properties of polymer-modified bitumen based on its morphology. *Road Materials and Pavement Design*, 18(S3):249-258. <https://doi.org/10.1080/14680629.2017.1329879>
- Wang P, Dong ZJ, Liu ZY, 2017b. Influence of carbon nanotubes on morphology of asphalts modified with styrene-butadiene-styrene. *Transportation Research Record*, 2632(1):130-139. <https://doi.org/10.3141/2632-14>
- Xu GJ, Wang H, 2016. Study of cohesion and adhesion properties of asphalt concrete with molecular dynamics simulation. *Computational Materials Science*, 112:161-169. <https://doi.org/10.1016/j.commatsci.2015.10.024>
- Xu GJ, Wang H, 2017. Molecular dynamics study of oxidative aging effect on asphalt binder properties. *Fuel*, 188:1-10. <https://doi.org/10.1016/j.fuel.2016.10.021>
- Xu GJ, Wang H, 2018. Diffusion and interaction mechanism of rejuvenating agent with virgin and recycled asphalt binder: a molecular dynamics study. *Molecular Simulation*, 44(17):1433-1443. <https://doi.org/10.1080/08927022.2018.1515483>
- Xu M, Yi JY, Feng DH, et al., 2016. Analysis of adhesive characteristics of asphalt based on atomic force microscopy and molecular dynamics simulation. *ACS Applied Materials & Interfaces*, 8(19):12393-12403. <https://doi.org/10.1021/acsami.6b01598>
- Yao H, Dai QL, You ZP, 2015. Chemo-physical analysis and molecular dynamics (MD) simulation of moisture susceptibility of nano hydrated lime modified asphalt mixtures. *Construction and Building Materials*, 101:536-547. <https://doi.org/10.1016/j.conbuildmat.2015.10.087>
- Yao H, Dai QL, You ZP, 2016. Molecular dynamics simulation of physicochemical properties of the asphalt model. *Fuel*, 164:83-93. <https://doi.org/10.1016/j.fuel.2015.09.045>
- Yu CH, Hu K, Yang QL, et al., 2021. Analysis of the storage stability property of carbon nanotube/recycled polyethylene-modified asphalt using molecular dynamics simulations. *Polymers*, 13(10):1658. <https://doi.org/10.3390/polym13101658>
- Zeng Q, Liu QC, Liu P, et al., 2020. Study on modification mechanism of nano-ZnO/polymerised styrene butadiene composite-modified asphalt using density functional theory. *Road Materials and Pavement Design*, 21(5):1426-1438. <https://doi.org/10.1080/14680629.2018.1552888>
- Zhang DM, Chen ZH, Zhang HL, et al., 2018. Rheological and anti-aging performance of SBS modified asphalt binders with different multi-dimensional nanomaterials. *Construction and Building Materials*, 188:409-416. <https://doi.org/10.1016/j.conbuildmat.2018.08.136>
- Zhang HL, Su MM, Zhao SF, et al., 2016. High and low temperature properties of nano-particles/polymer modified asphalt. *Construction and Building Materials*, 114:323-332. <https://doi.org/10.1016/j.conbuildmat.2016.03.118>
- Zhang HL, Gao Y, Guo GH, et al., 2018. Effects of ZnO particle size on properties of asphalt and asphalt mixture. *Construction and Building Materials*, 159:578-586. <https://doi.org/10.1016/j.conbuildmat.2017.11.016>
- Zhang LQ, Greenfield ML, 2007. Analyzing properties of model asphalts using molecular simulation. *Energy & Fuels*, 21(3):1712-1716. <https://doi.org/10.1021/ef060658j>
- Zhang LQ, Greenfield ML, 2008. Effects of polymer modification on properties and microstructure of model asphalt systems. *Energy & Fuels*, 22(5):3363-3375. <https://doi.org/10.1021/ef700699p>
- Zhou XX, Zhang GF, Liu RM, et al., 2014. Molecular simulations of anti-aging mechanisms on nano-LDHs modified asphalt. *Key Engineering Materials*, 599:198-202. <https://doi.org/10.4028/www.scientific.net/KEM.599.198>